ADVANCED MATERIALS INTERFACES
www.advmatinterfaces.de

A Novel Biasing Scheme of Electrolyte-Gated Organic Transistors for Safe In Vivo Amplification of Electrophysiological Signals

Michele Di Lauro, Elena Zucchini, Anna De Salvo, Emanuela Delfino, Michele Bianchi, Mauro Murgia, Stefano Carli, Fabio Biscarini, and Luciano Fadiga*

Successful translation of organic transistors as sensors and transducers to clinical settings is hampered by safety and stability issues. The operation of such devices demands driving voltages across the biotic/abiotic interface, which may result in undesired electrochemical reactions that may harm both the patient and the device. In this study, a novel operational mode is presented for electrolyte-gated organic transistors that avoid these drawbacks: the common-drain/grounded-source configuration. This approach reverts the standard common-source/common-ground configuration and achieves maximum signal amplification while applying null net bias across the electrolyte, with no parasitic currents. The viability of the proposed configuration is demonstrated by recording in vivo the somatosensory evoked activity from the barrel cortex of rats. The main inherent advantage of transistors with respect to passive electrodes is preserved in the proposed scheme: a superior signal-to-noise ratio is achieved which enables the detection of evoked activity at the single-trial level. Then, common-drain/grounded-source organic transistors are proposed as ideal candidate devices for a harmless translational recording platform.

1. Introduction

Recording of bioelectrical activity from the brain is widely adopted for both fundamental physiological investigation, e.g. the codification of superior activities as speech perception and production,[1–5] and clinical applications, such as intraoperative monitoring of neural activity during tumor resection neurosurgery,[6–8] identification of epileptic foci in chronic implants,[9–11] and neuroprosthetics.[12–17] In the effort to minimize invasiveness while preserving substantial task-related information, electrocorticographic (ECoG) and micro-electrocorticographic (μECoG) techniques underwent extensive investigation.[18–22] With respect to intracortical microelectrodes, both ECoG and μECoG exhibit some inherent limitation due to increased distance from the signal source.[23] Furthermore, μECoG suffers from noise enhancement due to electrode miniaturization and subsequent increased impedance.[24,25] In this scenario, brain recordings would highly benefit from an in situ first-stage signal amplification strategy. Among various strategies to overcome these limitations, semiconductor technology has been used in neurophysiological applications. Inorganic field-effect transistors were successfully demonstrated as transducers of bioelectrical activity in vitro,[26–28] yet their application in vivo is limited by the chemical and mechanical features of inorganic semiconductors, especially when exposed to aqueous environments.[29] This has relegated inorganic transistors to the role of integrated multiplexers for microelectrodes.[30]

M. Di Lauro, E. Zucchini, A. De Salvo, E. Delfino, M. Bianchi, M. Murgia, F. Biscarini, L. Fadiga
Center for Translational Neurophysiology of Speech and Communication
Fondazione Istituto Italiano di Tecnologia (IIT-CTNSC)
via Fossato di Mortara 17/19, Ferrara 44121, Italy
E-mail: michele.dilauro@iit.it

The ORCID identification number(s) for the author(s) of this article can be found under https://doi.org/10.1002/admi.202101798.

DOI: 10.1002/admi.202101798

E. Zucchini, A. De Salvo, E. Delfino, L. Fadiga
Sezione di Fisiologia
Dipartimento di Neuroscienze e Riabilitazione
Università di Ferrara
via Fossato di Mortara 17/19, Ferrara 44121, Italy

M. Murgia
Istituto per lo Studio dei Materiali Nanostrutturati (CNR-ISMN)
National Research Council
via Gobetti 101, Bologna 40129, Italy

S. Carli
Dipartimento di Scienze chimiche farmaceutiche ed agrarie
Università di Ferrara
via Luigi Borsari 46, Ferrara 44121, Italy

F. Biscarini
Dipartimento di Scienze della Vita
Università di Modena e Reggio Emilia
Via Campi 103, Modena 41125, Italy

Electrolyte-gated organic transistors (EGOTs) were successfully demonstrated as transducers in vivo,[31,32] since their working principle functionally integrates the electrolytic biological environment.[33,34] In these architectures, an organic (semi-)conductive channel is obtained by bridging two metal contacts, namely the source, S, and the drain, D, with a thin film of organic (semi-)conductor. A third electrode, named gate, G, sets the electrochemical potential of an electrolytic solution in physical contact with the channel, thereby controlling its conductivity.[33–37] In the classical common-source/common-ground configuration, a bias across the channel, V_{DS}, drives a channel current, I_{DS}. The bias between gate and source, V_{GS}, controls the ionic density in close proximity to the channel, thus modulating charge carrier density. The effect of V_{GS} manifests itself in the transconductance, g_m, defined as the derivative of I_{DS} with respect to V_{GS}, which quantifies the amplification capability of EGOTs. The most promising channel material for electrophysiological applications is poly(3,4-ethylenedioxythiophene):polystyrene sulfonate (PEDOT:PSS),[38] which enables to attain EGOTs with g_m in the mS range, high conductance in the ON state, and four-decade modulation of I_{DS} upon small $|V_{GS}|$ variations (<1 V). The low operational voltage arises from PEDOT:PSS extended electroactive surface area, that leads to a large effective capacitance.[39,40] Furthermore, PEDOT:PSS can be processed from aqueous formulations, is biocompatible and suitable for translation to human applications.[41–45]

As aforementioned, PEDOT:PSS-based EGOTs are normally operated in common-source/common-ground (CSCG) configuration, and electrophysiological applications do not represent an exception to this paradigm.[31,32] This implies that the drain electrode is negatively biased with respect to the source, as imposed by the positive sign of the charge carriers, while the gate electrode can be either negatively or positively biased, with respect to the same terminal, according to the desired doping-state of the channel. The resulting net potential between gate and drain, which roughly corresponds to V_{GS}–V_{DS}, widely exceeds the electrochemical stability window of water, thus undesired faradic reactions in the electrolyte may be activated. If this phenomenon represents a minor issue (and perhaps an advantage) in sensing applications,[46] it stands as a major drawback for translational electrophysiology since, in such a scenario, faradic reactions may elicit critical tissue damage because of the generation of chlorine and hydrogen at the electrodes.[47,48]

In this work, we propose and demonstrate a novel operation mode for EGOTs, aimed at avoiding the application of a bias in the brain while retaining the amplification features of the device architecture.

The new operation mode is simple: we revert the classical common-source/common-ground configuration to obtain a common-drain/grounded-source (CDGS) configuration. Across the channel, a positive V_{DS}, applied at the drain with respect to the grounded source, drives a positive hole current in the p-type conductor, while the potential of the gate electrode controlling the bath, V_{GD}, is referred to the drain itself and not to the source. In this setup, one achieves maximum transconductance in EGOTs when applying equal and opposite voltages at the drain (positive bias) and at the gate (negative bias), resulting in net zero bias in the cerebro-spinal fluid.

We tested the new CDGS configuration and compared it with the standard CSCG configuration, first at the benchside then in vivo, by performing electrophysiological recordings of somatosensory evoked activity from the cerebral cortex of anesthetized rats. During the whole duration of the recording session (several hours) no faradic current, event accidental, was flowing across the brain while the system showed optimal amplification performances. This demonstrates that the proposed recording scheme is safe for the living systems and remains functional for recording evoked activity with excellent signal-to-noise ratio (SNR).

2. Results and Discussion

EGOTs were fabricated as described in the Experimental Section and tested at the benchside in 1 M phosphate buffered saline.

Figure 1 depicts a detailed comparison between CSCG (Figure 1a) and CDGS (Figure 1g) architectures. In particular, it is worth noticing how, in terms of absolute values, both output (Figure 1b,h) and transfer (Figure 1d,j) characteristics are substantially independent of the adopted connection scheme. Nevertheless, in the proposed CDGS configuration, the *I*–*V* curves span the first and second quadrants ($I_{DS} > 0$ A) of the *I* versus *V* Cartesian plane (Figure 1h,j). Conversely, in the usual CSCG configuration, they span the third and fourth quadrants ($I_{DS} < 0$ A, Figure 1b,d). As expected for PEDOT:PSS channels, transfer characteristics exhibit depletion behavior and nonlinear dependence of transconductance, g_m, on gate voltage, with g_m saturating to its maximum value at negative V_{GS} or V_{GD}, for CSCG or CDGS, respectively. The maximum g_m regime is highlighted in Figure 1d,j.

Figure 1c,i schematically show how the driving voltages for CSCG and CDGS configurations span, illustrating how the maximum g_m regimes are achieved in profoundly different energetic layouts. In the CDGS configuration (Figure 1i), at the most negative V_{GD} value, the gate electrode—which sets the potential of the electrolyte—is equipotential with the ground. This is in stark contrast with what happens in CSCG (Figure 1c), where at the most negative V_{GS} value (i.e., at maximum g_m) the gate is negatively biased with respect to the ground, thus eliciting a net negative voltage in the bulk of the operational electrolyte. This results into the direct application of a bias to the brain in in vivo operations.

To quantitatively describe this crucial difference between the two configurations in terms of safety, the bulk electrolyte voltage, V_{bulk}, was probed with a bathing electrode, with the experimental layouts shown in Figure 1e,k. V_{bulk} values, acquired at constant V_{DS}, are shown in Figure 1f,l as a function of gate bias. In accordance with the discussion above, in the maximum g_m condition, V_{bulk} approaches –1 V in the standard CSCG configuration (Figure 1f), while it is null in the novel CDGS configuration (Figure 1l). Full V_{bulk} trends versus V_{DS} and either V_{GD} or V_{GS} are shown in Figure S1 (Supporting Information).

Then, EGOTs were acutely implanted in the barrel cortex of rats (**Figure 2**a) and performances of both architectures were assessed in vivo (Figure 2b). Anesthetized rats were positioned

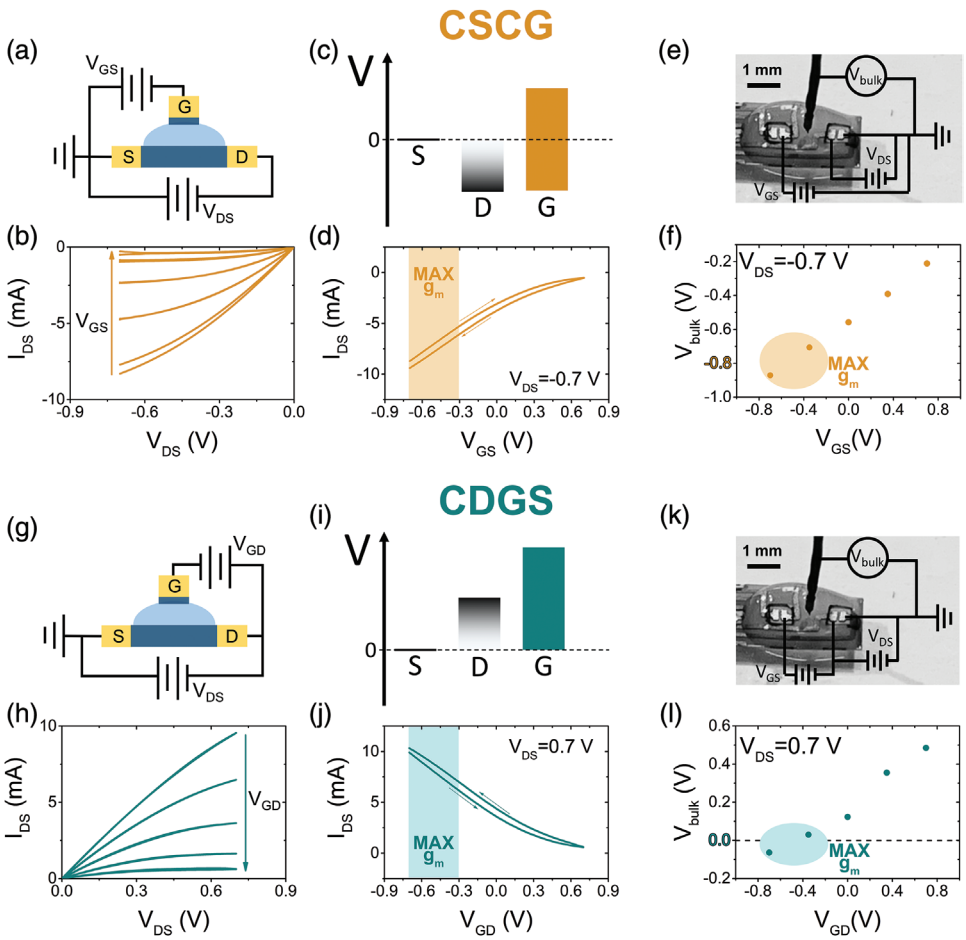

Figure 1. Benchside comparison of EGOT configuration. a) Connection layout of the common-source/common-ground (CSCG) EGOT. b) *I–V* output characteristics recorded in CSCG configuration scanning V_{DS} from –0.7 to 0.0 V at fixed V_{GS} values ranging from –0.7 to 0.7 V. Arrow indicates increasing V_{GS}. c) Schematic representation of the spans of the driving voltages in CSCG configuration. d) *I–V* transfer characteristic recorded in CSCG configuration scanning V_{GS} from –0.7 to 0.7 V at V_{DS} = –0.7 V. The maximum transconductance regime is highlighted. e) Photograph and circuit schematics of the V_{bulk} recording setup for CSCG EGOT. f) Scatter plot showing the dependence of V_{bulk} on V_{GS} in CSCG configuration, with highlighted maximum transconductance regime, showing strong negative V_{bulk} values at maximum transconductance. g) Connection layout of the common-drain/grounded-source (CDGS) EGOT. h) *I–V* output characteristics recorded in CDGS configuration scanning V_{DS} from 0.0 to 0.7 V at fixed V_{GD} values ranging from –0.7 to 0.7 V. Arrow indicates increasing V_{GD}. c) Schematic representation of the spans of the driving voltages in CDGS configuration. d) *I–V* transfer characteristic recorded in CDGS configuration scanning V_{GD} from –0.7 to 0.7 V at V_{DS} = 0.7 V. The maximum transconductance regime is highlighted. e) Photograph and circuit schematics of the V_{bulk} recording setup for CDGS EGOT. f) Scatter plot showing the dependence of V_{bulk} on V_{GD} in CDGS configuration, with highlighted maximum transconductance regime, showing null V_{bulk} at maximum transconductance.

in a stereotaxic apparatus and their sensorimotor cortex (barrel cortex representation of whiskers) was exposed by traditional neurosurgery procedure. Figure 2c reports an overlay of typical in vivo transfer characteristics, showing excellent agreement with the respective benchside *I–V* responses (cf., Figure 1d,j). In order to compare their recording capabilities, the two configurations were benchmarked against a well-defined potential modulation in the barrel cortex, the so-called somatosensory evoked potential (SEP).[49–51]

Such modulations were elicited by single-pulse mechanical stimulation of the rat whiskers and in situ amplified electrophysiological activity was acquired as I_{DS} versus time. Evidence of highly comparable in vivo performances of the two configurations is shown as mean I_{DS} profiles (Figure 2d) and quantified in terms of SNR (Figure 2e). For all the tested frequency bands, the ratio between the SNR of the CSCG EGOT and the SNR of the CDGS EGOT lays around value 1, hinting at identical amplification capabilities. The only noticeable difference is represented by the fact that the phases of the two I_{DS} responses to the same electric field modulation are reversed (Figure 2d), as implied by the opposite V_{DS} sign.

Focusing on the features of the neural activity collected with CDGS EGOTs, **Figure 3** reports an overview of the evoked signal acquired with the proposed architecture. As shown in Figure 3a, the mean I_{DS} profile depletes in roughly 75 ms after the stimulation onset and is characterized by two major peaks (a first negative peak and an almost equal amplitude positive peak), followed by a negative rebound. By looking at the I_{DS} spectrogram averaged over trials (Figure 3b), it is possible to appreciate the frequency content of such oscillation which exhibits relevant power up to 100 Hz. The features defining the event related current oscillation are extremely consistent in

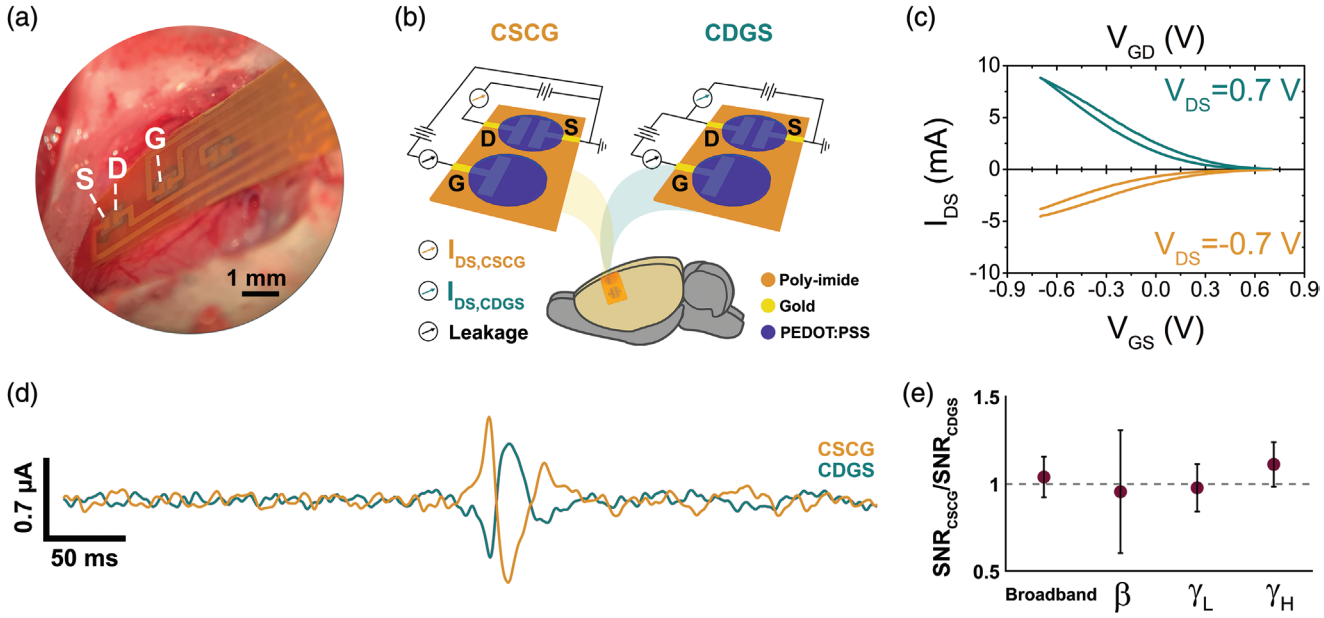

Figure 2. In vivo comparison of EGOT configurations. a) Photographic image of the device implanted over the rat barrel cortex. Labels identify source (S), drain (D), and gate (G) electrodes. b) Connection layouts of CSCG and CDGS EGOT configurations for in vivo recordings. c) In vivo transfer characteristics of both EGOT architectures (CSCG in yellow and CDGS in green). d) Averaged trials ($n = 100$) of the somatosensory evoked response collected with the two different configurations from the same cortical position (Rat 1). Data are time locked to the start of the whisker stimulation ($t = 0$ s) and band-pass filtered between 15 and 150 Hz. e) Scatter plot of the ratio between the SNR of the CSCG EGOT and the SNR of the CDGS EGOT (mean ± propagated SEM) calculated in all frequency bands (broadband 15–150 Hz; beta β 15–30 Hz; low-gamma γ_L 30–80 Hz; high-gamma γ_H 80–150 Hz).

different positions over the rat cortex as well as in different animals (Figure S2, Supporting Information).

This consistency is quantitatively investigated by computing the correlation between the average of trial subsets and the average of all trials. The aim is the determination of the minimum number of trials required to obtain a robust estimate of the somatosensory evoked response (Figure 3c). Using CDGS EGOTs, a single trial is sufficient to obtain a reliable representation (i.e., a correlation greater than 90%) of the average evoked response. This result is further corroborated by the collected raw traces (Figure S3, Supporting Information). Regardless of the offline data processing (i.e., data filtering), a clear post-stimulus peak stands out from the basal activity in all trials.

The in vivo amplification capability of the proposed architecture was assessed by comparing the recorded I_{DS} traces with voltage traces, V_{El}, collected with a standard electrophysiological *apparatus*. In the latter configuration, the gate terminal is used as a passive recording electrode, which collects SEPs as voltage fluctuations with respect to a reference point (a grounded small screw placed on the skull). **Figure 4**a,b shows current and voltage traces for the same rat in the same position. Noticeably, a phase reversal is observed between voltage and current traces. In particular, the two peaks (first positive, then negative) of the potential of the gate electrode, when used as a passive recording site (Figure 4b), and the two opposite peaks in EGOT I_{DS} (Figure 4a) is due to the fact that a positive shift of the gate voltage with respect to the ground (i.e., the source) results in a less negative V_{GD}. In our configuration, less negative V_{GD} corresponds to a lower doping level, providing a lower positive current (Figure 1j and 2c) and, hence, a negative I_{DS} peak. This phase reversal is not observed in CSCG configuration (Figure 2d), where a lower doping level corresponds to a lower negative current (Figure 1d and 2c) and to a positive I_{DS} peak.

The amplitude of EGOT-transduced signals is consistent with the EGOT working principle, since a voltage variation of 100 µV gives rise to a current variation of 1 µA, coherently with the g_m values in the 10 mS range, as in the I–V characteristics of such devices (Figure 1d,j and 2c).

A direct comparison between the performances of electrode (i.e., voltage) and CDGS EGOT (i.e., current) recordings is given in terms of the SNR, as described in the Experimental Section. Figure 4c shows SNRs of I_{DS} and V_{El} recordings for the whole investigated bandwidth (15–150 Hz) and for individual frequency bands (β 15–30 Hz, γ_{Low} 30–80 Hz and γ_{High} 80–150 Hz). It is evident the marked gain in SNR yielded by the CDGS EGOT architecture compared to the passive electrode (Figure 4c). Due to the well-known gain/bandwidth tradeoff of EGOTs,[40] this gain scales inversely with the increase of frequency.

From the correlation analysis of the voltage traces it is possible to notice that the minimum trial number to obtain a reliable estimate of the SEP increases to 3 when recording with passive electrodes (Figure S4, Supporting Information).

An additional in vivo experiment aimed at comparing stimulated, spontaneous, and after-sacrifice activity was performed to further investigate the recording capabilities of the proposed EGOT operational mode. As shown in **Figure 5**, it is possible to appreciate a marked difference among these three conditions, both in time (Figure 5a) and time–frequency domains (Figure 5b). As expected, I_{DS} recorded during stochastic whisker stimulation shows bursts of activity up to 150 Hz which stand out with respect to basal current oscillations and

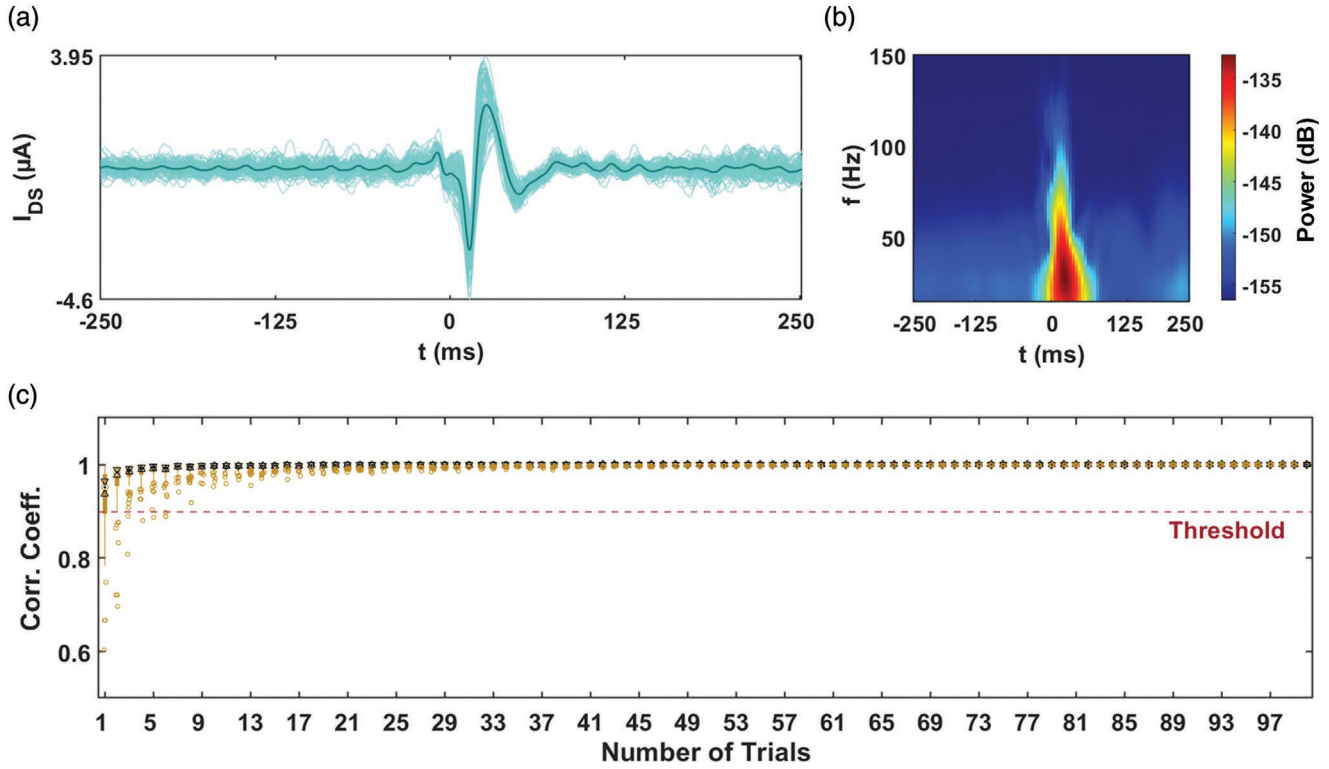

Figure 3. Transduction of somatosensory evoked response recorded with CDGS EGOT. a) Average (dark green, $n = 100$, Rat 2, Position 2) and single trials (light green) of the somatosensory evoked responses, time locked to the start of the whisker stimulation ($t = 0$ s) measured as I_{DS} versus time. Data are band-pass filtered between 15 and 150 Hz. b) Average ($n = 100$, Rat 2, Position 2) spectrogram of I_{DS}. c) Box-plots (in yellow) of the correlation coefficient values computed between I_{DS} averaged over 100 randomly selected trial groups and I_{DS} averaged over all trials ($n = 100$), iterated increasing group numerosity by steps of 1, reported versus group numerosity. Dashed red line indicates the selected threshold to achieve a reliable estimation of the somatosensory evoked response. Here minimum trial number to obtain a correlation higher than 90% is 1.

are absent few minutes after sacrificing the animals by means of an intracardiac injection of Tanax. Such a drastic increase is quantitatively visualized by the spectrograms; indeed, the power of the spontaneous activity represents the 22% of the power of the stimulated activity. Moreover, the *post mortem* recordings, exhibit power as low as 3% of the stimulated signal power, showing a very low level of noise of the device when not exposed to biological electrical signals.

To convert I_{DS} signals in voltage variations, we simulated the voltage traces, V_{out}, that would be output by an EGOT with the readout circuit depicted in **Figure 6**a, where a load resistor, R_L, equal to the average channel resistance, is placed in series with the channel. Figure 6c shows the simulated EGOT V_{out}, which, by definition, would exhibit the same superior SNR of current measurements (Figure 4c) with respect to V_{El} (Figure 4b). Nonetheless, the experimental recording of V_{out} demands the addition of a filtering stage, since the resting V_{out} is offset by a factor $\approx V_{DS}/2$ (i.e., −350 mV in our case), which widely exceeds the maximum voltage input of standard electrophysiological pre-amplifiers (i.e., ±10 mV in our TDT PZ2 described in the Experimental Section). Figure 6d shows the experimental voltage, V_{exp}, as output by the circuit designed in Figure 6b, which includes a high-pass filter at 10 Hz. As shown by the comparison between Figure 6c,d, the addition of a stage which includes ohmic components results in an increased noise, undermining the SNR gain provided by EGOT architecture.

3. Conclusions and Perspectives

The herein presented common-drain/grounded-source EGOT overcomes a critical problem of translational organic bioelectronics, namely the application of a potentially harmful bias to tissues and bodily fluids. Earlier attempts to overcome this issue in the classical common-source/common-ground configuration focused on achieving maximum transconductance at $V_{GS} = 0$ V, thereby posing strict fabrication constraints.[52] In the common-drain/grounded-source layout, driving voltages at the gate and at the drain can be adjusted to achieve maximum transconductance in order to cope with various device geometries and application scenarios, without compromising the safety of EGOT operation in the brain and its recording capabilities.

Notably, due to the high channel conductance of PEDOT:PSS EGOTs, important event-related current variations do not imply significant resistance changes, hence V_{out} values with voltage divider readout strategies do not show any gain with respect to recording techniques based on passive electrodes, albeit theoretically retaining the superior SNR of EGOTs. For this reason, in the literature, it has been proposed to couple EGOTs with a second stage operational low-noise amplifier to convert current to voltage (mimicking a grounded inductor), thereby boosting V_{out} amplitude.[53] Although effective, this approach partially undermines the *raison d'etre* of EGOTs as in situ amplifiers, since it implies the integration of an ex situ amplification circuitry. Conversely,

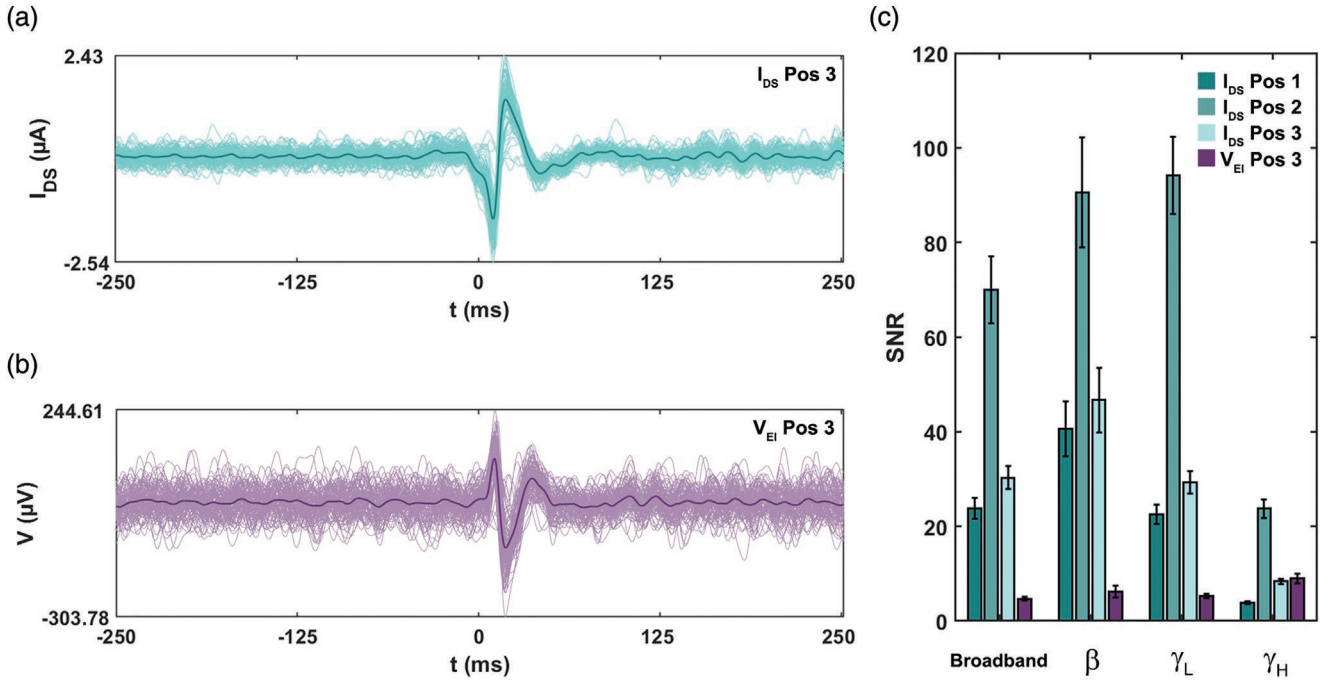

Figure 4. Comparison between current and voltage recordings. a) Average (dark green, $n = 100$, Rat 3, Position 3) and single trials (light green) of the somatosensory evoked responses, time locked to the start of the whisker stimulation ($t = 0$ s) measured as I_{DS} versus time. Data are band-pass filtered between 15 and 150 Hz. b) Average (dark purple, $n = 100$, Rat 2, Position 3) and single trials (light purple) of the somatosensory evoked responses, time locked to the start of the whisker stimulation ($t = 0$ s) measured as voltage versus time. Data are band-pass filtered between 15 and 150 Hz. c) Bar plot of the SNR values (mean ± SEM) calculated in all frequency bands (broadband 15–150 Hz; beta β 15–30 Hz; low-gamma γ_L 30–80 Hz; high-gamma γ_H 80–150 Hz) for all the recording sessions.

we highlight that, to make full use of the advantages provided by EGOTs as electrophysiological transducers, one should adopt recording methods that directly use channel current as readout rather than forcing EGOT architectures into classical electrophysiology systems at the price of losing part of their benefits.

Examples of these benefits are the more-than-tenfold higher SNR with respect to passive electrodes (Figure 4c) and the capability of recognizing the event at a single trial level (Figure 3c). Both are essential features in view of the effective deployment of brain computer interfaces (BCIs), that are exposed to a continuous flow of different neural information that needs to be resolved in real time. The EGOT common-drain/grounded-source operational mode we propose here enables the safe translation of both high SNR and event recognition at the single-trial level to clinical scenarios and may constitute a stepping-stone toward translational organic bioelectronics.

4. Experimental Section

Device Fabrication: Test patterns were custom-designed and purchased by Phoenix PCB (Ivrea, Italy). The final design featured two independent pairs of gold source/drain electrodes ($W/L = 4$) patterned onto a flexible poly-imide substrate. Insulation was guaranteed by a further poly-imide layer which covered the entire layout and featured two pools which exposed only the terminal portion of the source and drain leads (area = 0.8 mm × 0.9 mm). PEDOT:PSS films were obtained by drop-casting 0.5 μL of a PEDOT:PSS formulation (Clevios PH1000, 5% v/v DMSO, 0.2% v/v GOPS; diluted ten times with MilliQ water) on

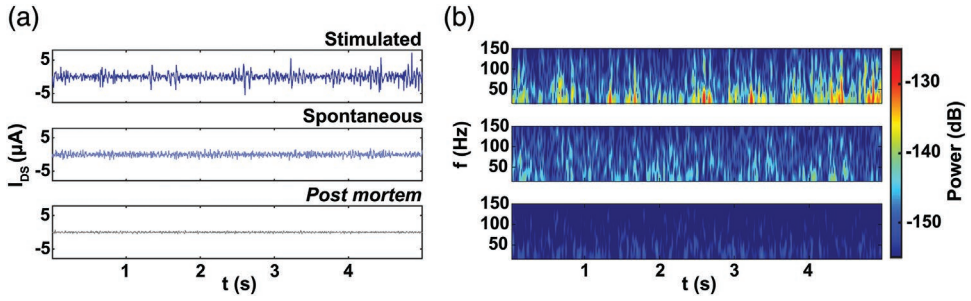

Figure 5. Recording capabilities of CDGS EGOT. a) I_{DS} recordings of stimulated (top), spontaneous (center) and *post mortem* (bottom) activity, in a 5 s time window (Rat 4). Data are band-pass filtered between 15 and 150 Hz. b) Spectrograms comparing the stimulated (top), spontaneous (center), and *post mortem* (bottom) activity in the time–frequency domain.

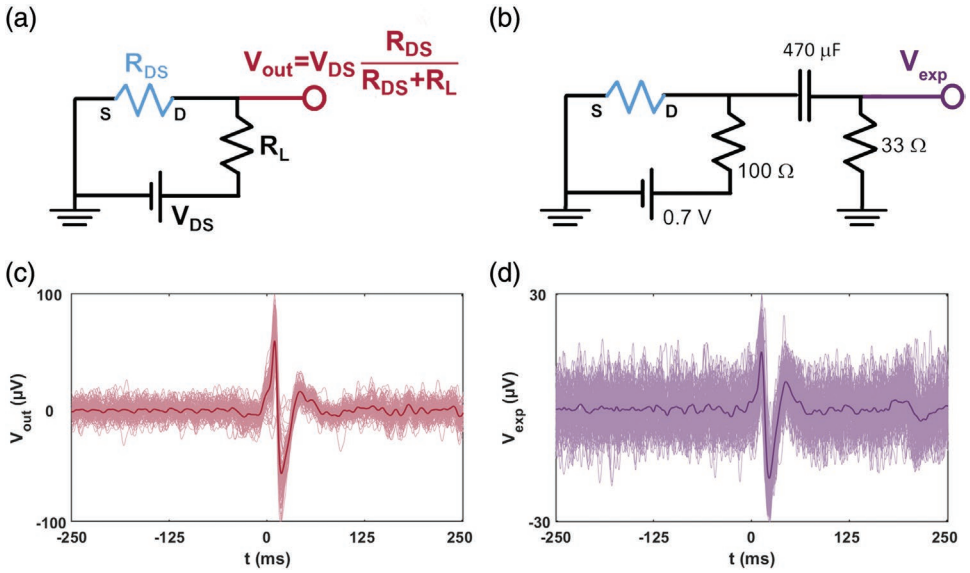

Figure 6. Voltage divider readout strategy. a) Theoretical readout circuit enabling conversion of I_{DS} signal into a voltage variation. R_L is set equal to R_{DS}, computed as $V_{DS}/2I_{DS}$. b) Experimental readout circuit, with the addition of a high-pass RC filter at 10 Hz. c) Average (dark red, $n = 100$, Rat 3, Position 3) and single trials (light red) of the simulated V_{out} signals, time locked to the start of the whisker stimulation ($t = 0$ s). Data are band-pass filtered between 15 and 150 Hz. d) Average (dark purple, $n = 100$, Rat 1) and single trials (light purple) of the recorded V_{exp} signals, time locked to the start of the whisker stimulation ($t = 0$ s). Data are band-pass filtered between 15 and 150 Hz.

each pool and curing in a thermostatic oven (120 °C, 30 min) obtaining films with an average 1 µm thickness (XE7 AFM Park System, tapping mode), following a previously published protocol.[54] The two leads in one pool were used as source and drain contacts, while the two leads in the other pool were short circuited, resulting in a single PEDOT:PSS surface gate electrode.

In Vivo Recordings on Rats: Experiments were performed in compliance with the guidelines established by the European Communities Council (Directive 2010/63/EU, Italian Legislative Decree n. 26, 4/3/2014) and the protocol was approved by the Ethics Committee for animal research of the University of Ferrara and by the Italian Ministry of Health (permission n. 989/2020-PR).

EGOTs were assessed in vivo on four adult Long Evans rat (males, 400–500 g) on the primary somatosensory cortex (barrel field), S1BF.[55] The surgical procedure to expose the rat barrel cortex, implant the device, and mechanically elicit somatosensory evoked responses (SEPs) was performed using the same protocols described elsewhere.[42,56,57]

Briefly, the animals were anesthetized with a mixture of Zoletil (Virbac, France; 30 mg kg^{-1}) and Xylazine (Bayer, Germany; 5 mg kg^{-1}) administered intraperitoneally (i.p.). For the entire duration of the procedure, the depth of anesthesia was monitored by testing the absence of hind limb withdrawal reflex and was maintained by additional intramuscular (i.m.) doses of anesthetic. The anesthetized animals were then placed in a stereotaxic apparatus (David Kopf Instruments, USA) equipped with ear bars (Model 957 for small animals) and a ≈ 2 cm long incision was made along the midline of the cranium. The underlying muscle and connective tissue were retracted to expose the skull and a craniotomy (≈ 6 × 6 mm^2) was performed in the parietal bone to expose the somatosensory cortex, identified according to vascular landmarks and stereotaxic coordinates.[55] Sterile saline solution was applied while drilling to avoid any local heating and to keep the bone surface clean. A stainless steel bone screw was inserted in the contralateral parietal bone serving, when needed, as ground/reference point. Finally, each device was placed epidurally over the barrel cortex.[55]

To elicit the neural response of the rat barrel cortex, a vibrating system was used to produce a multiwhiskers deflection along the horizontal plane. Rats whiskers contralateral to the craniotomy were shortened and inserted in a Velcro strip attached to a rod moved by a shaker (Type 4810 mini shaker, Bruel & Kjaer, Denmark) controlled by a National Instruments board (Austin, USA). The deflection stimulus, consisting of a sine waveform of 12 ms duration and an amplitude coincident with whiskers deflection of 500 µm, was repeated 100 times.

Neural data were acquired at 2000 samples s^{-1} using a Keysight B2912A Source-Measure Unit with the biasing scheme reported in Figure 1. To reduce electromagnetic noise, the recorded animals were placed in a Faraday cage. Maximum transconductance was achieved by applying $V_{GD} = -0.7$ V and $V_{DS} = 0.7$ V, resulting in net zero bias in the brain.

When aiming to collect somatosensory evoked responses (1 position over the cortex of Rat 1, 2 positions over the cortex of Rat 2 and 1 position over the cortex of Rat 3), 1 s trials ($n = 100$), triggered by the start of the whiskers stimulation, were collected. Differently, as a further assessment of the recording capability of EGOT (Rat 4), 5 s recording sessions were collected during stochastic mechanical stimulation of the rat whiskers, during spontaneous neural activity without stimulation, and after sacrificing the animals with an intracardiac injection of Tanax (0.3 mL kg^{-1}).

Voltage recordings of SEPs employing the gate EGOT terminal as a passive electrode were performed using a Tucker Davis Technologies multichannel recording system 3 (Tucker Davis Technologies, USA) including: the ZIF-Clipheadstage with unity (1X) gain, the RZ2 real-time processor, and the PZ2-256 battery-powered preamplifier. Data were digitized at a sample rate of 12 207 samples s^{-1} and transferred from the RZ2 processor to a computer by fast fiber optic connection. As required by the single-ended headstage configuration, reference and ground pins of the headstage were tied together and connected to a screw placed on the skull.

Data Analysis: Neural data analysis was carried out using Matlab (version 9.10, Mathworks, Natick, MA, USA). All the recorded signals were band-pass filtered (15–150 Hz, by the Matlab function *filtfilt*, 4th order Butterworth). Additionally, AC line noise was removed with a 50 Hz notch filter (4th order Butterworth). Voltage traces (sampling frequency = 12 207 samples s^{-1}) were undersampled at 2000 samples s^{-1} prior to filtering, for comparison purposes with the current traces.

Neural activity in both time and time-frequency domains evoked by whiskers stimulation was compared to spontaneous activity in the absence of stimulation and to the noise level of the system (i.e., current acquired after sacrificing the animals). Specifically, to examine the data in the time-frequency domain, the Matlab function *spectrogram* was used setting a window length of 100 samples and 90% of window overlap. The power of the signals recorded in the three different conditions was estimated as the square of the RMS level using the Matlab function *bandpower* in the 15–150 Hz frequency range.

To investigate the somatosensory evoked responses recorded with EGOTs and passive electrodes, data were segmented (500 ms window, centered on stimulus onset). The mean over trials was computed in the time domain and the average spectrogram was calculated as aforementioned (window length of 100 samples, 90% overlap).

The SNR was calculated as the ratio between the power of the event (i.e., the power in the 75 ms time window after the start of the stimulation) and the power of an equally wide time window of pre-stimulus spontaneous activity, as previously reported for the analysis of event related potentials (ERP).[42,58,59]

The correlation between either I_{DS} or V_{EI} averaged over 100 randomly selected trial groups and the average over all trials was computed to determine the minimum number of trials required to obtain a robust estimate of the somatosensory evoked response. Correlation coefficients were computed using the Matlab function *corrcoef* in a time window of 75 ms after the stimulation onset. The procedure was repeated increasing group numerosity by steps of 1 until reaching the total amount of collected trials (n = 100). A correlation of 90% was set as threshold to determine the number of trials required to obtain a reliable estimation of the somatosensory evoked response.[58]

Supporting Information

Supporting Information is available from the Wiley Online Library or from the author.

Acknowledgements

M.D.L. and E.Z. contributed equally to this work. F.B. and L.F. contributed equally to this work. Research work leading to this publication was funded by IIT—Istituto Italiano di Tecnologia, University of Ferrara and University of Modena and Reggio Emilia (FAR 2018 Project e-MAP).

Open Access Funding provided by Istituto Italiano di Tecnologia within the CRUI-CARE Agreement.

Conflict of Interest

The authors declare no conflict of interest.

Data Availability Statement

The data that support the findings of this study are available from the corresponding author upon reasonable request.

Keywords

common-drain/grounded-source, conducting polymers, electrocorticography, electrolyte-gated organic transistors, in vivo electrophysiology, organic bioelectronics

Received: September 18, 2021
Revised: January 18, 2022
Published online: March 3, 2022

[1] D. Conant, K. E. Bouchard, E. F. Chang, *Curr. Opin. Neurobiol.* **2014**, *24*, 63.
[2] K. E. Bouchard, N. Mesgarani, K. Johnson, E. F. Chang, *Nature* **2013**, *495*, 327.
[3] E. F. Chang, D. D. Wang, D. W. Perry, N. M. Barbaro, M. S. Berger, *J. Neurosurg.* **2011**, *114*, 893.
[4] N. E. Crone, A. Sinai, A. Korzeniewska, in *Event-Related Dynamics of Brain Oscillations* (Eds: C. Neuper, W. Klimesch), Elsevier, Amsterdam **2006**, p. 275.
[5] E. F. Chang, J. W. Rieger, K. Johnson, M. S. Berger, N. M. Barbaro, R. T. Knight, *Nat. Neurosci.* **2010**, *13*, 1428.
[6] P.-S. Yao, S.-F. Zheng, F. Wang, D.-Z. Kang, Y.-X. Lin, *J. Neurosurg.* **2017**, *128*, 840.
[7] G. Bertani, E. Fava, G. Casaceli, G. Carrabba, A. Casarotti, C. Papagno, A. Castellano, A. Falini, S. M. Gaini, L. Bello, *Neurosurg. Focus* **2009**, *27*, E4.
[8] G. Ojemann, *Intraoperative Monitoring in Epilepsy* (Eds: A. M. Lozano, P. L. Gildenberg, R. R. Tasker), Springer, Berlin **2009**, pp. 2651.
[9] N. J. Hill, D. Gupta, P. Brunner, A. Gunduz, M. A. Adamo, A. Ritaccio, G. Schalk, *J. Visualized Exp.* **2012**, 1.
[10] A. Y. Chan, R. C. Knowlton, E. F. Chang, V. R. Rao, *Clin. Neurophysiol. Pract.* **2018**, *3*, 174.
[11] D. J. DiLorenzo, E. Z. Mangubat, M. A. Rossi, R. W. Byrne, *J. Neurosurg.* **2014**, *120*, 1402.
[12] S. Micera, *Nat. Biomed. Eng.* **2017**, *1*, 73.
[13] P. Romanelli, M. Piangerelli, D. Ratel, C. Gaude, T. Costecalde, C. Puttilli, M. Picciafuoco, A. Benabid, N. Torres, *J. Neurosurg.* **2018**, *130*, 1166.
[14] S. Martin, I. Iturrate, J. d. R. Millán, R. T. Knight, B. N. Pasley, *Front. Neurosci.* **2018**, *12*, 422.
[15] K. Volkova, M. A. Lebedev, A. Kaplan, A. Ossadtchi, *Front. Neuroinf.* **2019**, *13*, 74.
[16] G. Schalk, E. C. Leuthardt, *IEEE Rev. Biomed. Eng.* **2011**, *4*, 140.
[17] Q. Rabbani, G. Milsap, N. E. Crone, *Neurotherapeutics* **2019**, *16*, 144.
[18] W. Wang, A. D. Degenhart, D. L. Holder, S. Louis, D. W. Moran, S. Louis, In 2009 Annual International Conference of the IEEE Engineering in Medicine and Biology Society, **2009**, pp. 586.
[19] S. Kellis, L. Sorensen, F. Darvas, C. Sayres, K. O'Neill, R. B. Brown, P. House, J. Ojemann, B. Greger, *Clin. Neurophysiol.* **2016**, *127*, 591.
[20] R. Vinjamuri, D. J. Weber, A. D. Degenhart, J. L. Collinger, G. P. Sudre, P. D. Adelson, D. L. Holder, M. L. Boninger, A. B. Schwartz, D. J. Crammond, E. C. Tyler-Kabara, W. Wang, in *2009 Annu. Int. Conf. IEEE Engineering in Medicine and Biology Society*, **2009**, pp. 4339.
[21] K. J. Miller, E. C. Leuthardt, G. Schalk, R. P. N. Rao, N. R. Anderson, D. W. Moran, J. W. Miller, J. G. Ojemann, *J. Neurosci.* **2007**, *27*, 2424 LP.
[22] A. Gunduz, P. Brunner, A. Daitch, E. C. Leuthardt, A. L. Ritaccio, B. Pesaran, G. Schalk, *Front. Hum. Neurosci.* **2011**, *5*, 89.
[23] G. Buzsáki, C. A. Anastassiou, C. Koch, *Nat. Rev. Neurosci.* **2012**, *13*, 407.
[24] S. F. Cogan, *Annu. Rev. Biomed. Eng.* **2008**, *10*, 275.
[25] A. Ansaldo, E. Castagnola, E. Maggiolini, L. Fadiga, D. Ricci, *ACS Nano* **2011**, *5*, 2206.
[26] P. Fromherz, *Solid-State Electron.* **2008**, *52*, 1364.
[27] Q. Qing, S. K. Pal, B. Tian, X. Duan, B. P. Timko, T. Cohen-Karni, V. N. Murthy, C. M. Lieber, *Proc. Natl. Acad. Sci. USA* **2010**, *107*, 1882.
[28] P. B. Kruskal, Z. Jiang, T. Gao, C. M. Lieber, *Neuron* **2015**, *86*, 21.
[29] L. Yin, A. B. Farimani, K. Min, N. Vishal, J. Lam, Y. K. Lee, N. R. Aluru, J. A. Rogers, *Adv. Mater.* **2015**, *27*, 1857.
[30] C. H. Chiang, S. M. Won, A. L. Orsborn, K. J. Yu, M. Trumpis, B. Bent, C. Wang, Y. Xue, S. Min, V. Woods, C. Yu, B. H. Kim, S. B. Kim, R. Huq, J. Li, K. J. Seo, F. Vitale, A. Richardson, H. Fang, Y. Huang, K. Shepard, B. Pesaran, J. A. Rogers, J. Viventi, *Sci. Transl. Med.* **2020**, *12*, eaay4682.

[31] D. Khodagholy, T. Doublet, P. Quilichini, M. Gurfinkel, P. Leleux, A. Ghestem, E. Ismailova, T. Hervé, S. Sanaur, C. Bernard, G. G. Malliaras, *Nat. Commun.* **2013**, *4*, 1575.
[32] C. Cea, G. D. Spyropoulos, P. Jastrzebska-Perfect, J. J. Ferrero, J. N. Gelinas, D. Khodagholy, *Nat. Mater.* **2020**, *19*, 679.
[33] M. Di Lauro, M. Berto, M. Giordani, S. Benaglia, G. Schweicher, D. Vuillaume, C. A. Bortolotti, Y. H. Geerts, F. Biscarini, *Adv. Electron. Mater.* **2017**, *3*, 1700159.
[34] J. T. Friedlein, R. R. McLeod, J. Rivnay, *Org. Electron.* **2018**, *63*, 398.
[35] D. A. Bernards, G. G. Malliaras, *Adv. Funct. Mater.* **2007**, *17*, 3538.
[36] M. Di Lauro, S. la Gatta, C. A. Bortolotti, V. Beni, V. Parkula, S. Drakopoulou, M. Giordani, M. Berto, F. Milano, T. Cramer, M. Murgia, A. Agostiano, G. M. Farinola, M. Trotta, F. Biscarini, *Adv. Electron. Mater.* **2020**, *6*, 1900888.
[37] M. Di Lauro, S. Casalini, M. Berto, A. Campana, T. Cramer, M. Murgia, M. Geoghegan, C. A. Bortolotti, F. Biscarini, M. Di Lauro, S. Casalini, M. Berto, A. Campana, T. Cramer, M. Murgia, M. Geoghegan, C. A. Bortolotti, F. Biscarini, R. Emilia, V. G. Campi, *ACS Appl. Mater. Interfaces* **2016**, *8*, 31783.
[38] A. Elschner, S. Kirchmeyer, W. Lövenich, U. Merker, K. Reuter, *PEDOT: Principles and Applications of an Intrinsically Conductive Polymer*, CRC Press, Boca Raton, FL **2010**.
[39] M. Bianchi, S. Carli, M. Di Lauro, M. Prato, M. Murgia, L. Fadiga, F. Biscarini, *J. Mater. Chem. C* **2020**, *8*, 11252.
[40] J. Rivnay, P. Leleux, M. Ferro, M. Sessolo, A. Williamson, D. A. Koutsouras, D. Khodagholy, M. Ramuz, X. Strakosas, R. M. Owens, C. Benar, J. M. Badier, C. Bernard, G. G. Malliaras, *Sci. Adv.* **2015**, *1*, e1400251.
[41] M. Vomero, E. Castagnola, J. S. Ordonez, S. Carli, E. Zucchini, E. Maggiolini, C. Gueli, N. Goshi, F. Ciarpella, C. Cea, L. Fadiga, D. Ricci, S. Kassegne, T. Stieglitz, *Adv. Biosyst.* **2018**, *2*, 1700081.
[42] M. Vomero, E. Castagnola, F. Ciarpella, E. Maggiolini, N. Goshi, E. Zucchini, S. Carli, L. Fadiga, S. Kassegne, D. Ricci, *Sci. Rep.* **2017**, *7*, 40332.
[43] D. Khodagholy, J. N. Gelinas, Z. Zhao, M. Yeh, M. Long, J. D. Greenlee, W. Doyle, O. Devinsky, G. Buzsáki, *Sci. Adv.* **2016**, *2*, e1601027.
[44] M. Asplund, E. Thaning, J. Lundberg, A. C. Sandberg-Nordqvist, B. Kostyszyn, O. Inganäs, H. von Holst, *Biomed. Mater.* **2009**, *4*, 045009.
[45] D. Khodagholy, J. N. Gelinas, T. Thesen, W. Doyle, O. Devinsky, G. G. Malliaras, G. Buzsáki, *Nat. Neurosci.* **2015**, *18*, 310.
[46] M. Berto, C. Diacci, L. Theuer, M. Di Lauro, D. T. Simon, M. Berggren, F. Biscarini, V. Beni, C. A. Bortolotti, *Flexible Printed Electron.* **2018**, *3*, 24001.
[47] H. K. Abdel-Aal, I. A. Hussein, *Int. J. Hydrogen Energy* **1993**, *18*, 485.
[48] H. K. Abdel-Aal, S. M. Sultan, I. A. Hussein, *Int. J. Hydrogen Energy* **1993**, *18*, 545.
[49] M. E. Diamond, M. von Heimendahl, P. M. Knutsen, D. Kleinfeld, E. Ahissar, *Nat. Rev. Neurosci.* **2008**, *9*, 601.
[50] C. C. H. Petersen, *Neuron* **2007**, *56*, 339.
[51] C. C. H. Petersen, *Nat. Rev. Neurosci.* **2019**, *20*, 533.
[52] J. Rivnay, P. Leleux, M. Sessolo, D. Khodagholy, T. Hervé, M. Fiocchi, G. G. Malliaras, *Adv. Mater.* **2013**, *25*, 7010.
[53] P. Sideris, *Ph.D. Thesis*, Aristotle University of Thessaloniki **2016**.
[54] M. Di Lauro, A. De Salvo, G. C. Sebastianella, M. Bianchi, S. Carli, M. Murgia, L. Fadiga, F. Biscarini, *ACS Appl. Electron. Mater.* **2020**, *2*, 1849.
[55] G. Paxinos, C. Watson, *The Rat Brain in Stereotaxic Coordinates*, London Academic Press, London **2009**.
[56] M. Vomero, E. Zucchini, E. Delfino, C. Gueli, N. C. Mondragon, S. Carli, L. Fadiga, T. Stieglitz, *Materials* **2018**, *11*, 2486.
[57] M. Vomero, C. Gueli, E. Zucchini, L. Fadiga, J. B. Erhardt, S. Sharma, T. Stieglitz, *Adv. Mater. Technol.* **2020**, *5*, 1900713.
[58] X. Mike, Cohen, *Analyzing Neural Time Series Data: Theory and Practice*, MIT Press, Cambridge, MA **2014**.
[59] A. Suarez-Perez, G. Gabriel, B. Rebollo, X. Illa, A. Guimerà-Brunet, J. Hernández-Ferrer, M. T. Martínez, R. Villa, M. V. Sanchez-Vives, *Front. Neurosci.* **2018**, *12*, 00862.